References

BHAGAVANTAM, S. (1966). *Crystal Symmetry and Physical Properties.* New York: Academic Press.

BHAGAVANTAM, S. & PANTULU, P. V. (1964). *Proc. Indian Acad. Sci.* 59A, 1-13.

BHAGAVANTAM, S. & SURYANARAYANA, D. (1949). *Acta Cryst.* 2, 21-26.

BHAGAVANTAM, S. & VENKATARAYUDU, T. (1951). *Theory of Groups and its Application to Physical Problems.* Waltair: Andhra Univ. Press.

CHELAM, E. V. (1961). PhD Thesis. Indian Institute of Science, Bangalore, India.

INDENBOM, V. L., BELOV, N. V. & NERONOVA, N. N. (1960). *Kristallografiya,* 5, 497-500. [*Sov. Phys. Crystallogr.* (1961), 5, 477-481.]

JAHN, H. A. (1949). *Acta Cryst.* 2, 30-33.

KRISHNAMURTY, T. S. G. (1963). *Acta Cryst.* 16, 839-840.

KRISHNAMURTY, T. S. G. & GOPALA KRISHNA MURTY, P. (1968). *Acta Cryst.* A24, 563-564.

NYE, J. F. (1985). *Physical Properties of Crystals.* Oxford: Clarendon Press.

RAMA MOHANA RAO, K. (1985). *J. Phys. A,* 18, 739-748.

RAMA MOHANA RAO, K. (1987). *J. Phys. A,* 20, 47-57.

RAMA MOHANA RAO, K. (1988). *J. Phys. A,* 21, 1513-1518.

ROMAN, T. (1959). *Dokl. Akad. Nauk SSSR,* 128, 1122-1124.

TISZA, L. (1933). *Z. Phys.* 82, 48-72.

WOOSTER, W. A. (1979). *Tensors and Group Theory for the Physical Properties of Crystals.* Oxford: Clarendon Press.

ZAMORZAEV, A. M. (1963). *Kristallografiya,* 8, 307-312. [*Sov. Phys. Crystallogr.* (1963), 8, 241-245.]

Analysis of Neutron Diffraction Data in the Case of High-Scattering Cells

BY C. PETRILLO

Istituto di Struttura della Materia del Consiglio Nazionale delle Ricerche, Via Enrico Fermi 38, 00044 Frascati, Italy

AND F. SACCHETTI

Dipartimento di Fisica dell'Università di Perugia, Perugia, Italy

Abstract

A data reduction procedure is presented to analyse neutron diffraction intensities from low-scattering-power systems contained in high-scattering cells. A careful analysis of the cell contribution is carried out and a numerical program to treat absorption and multiple scattering also due to the cell is developed.

1. Introduction

The purpose of a neutron diffraction experiment from non-crystalline samples is to obtain the static structure factor $S(Q)$ from the measured intensity. However, the scattered neutron flux contains some background (scattering from container and environment) and is affected by absorption, multiple processes and inelasticity contributions apart from instrumental effects like beam inhomogeneity, counter efficiency and resolution.

In the case of high-scattering-power samples or for low container contribution to the total scattered intensity, the data reduction can be done by following standard procedures like that outlined by Paalman & Pings (1962) after a subtraction of the multiple scattering due to the sample only according to Blech & Averbach (1965). On the other hand, when such experimental conditions do not prevail, *i.e.* when the container contribution is an appreciable fraction of the total measured intensity (over 10%), the simplifying approximation of a negligible-thickness cell in evaluating the multiple scattering no longer holds.

One of the most widely employed approaches to the problem of multiple scattering from the sample and/or the container makes use of Monte Carlo (MC) procedures (Bischoff, Yeater & Moore, 1972; Copley, 1974, 1981; Copley, Verkerk, van Well & Fredrikze, 1986; Meardon, 1973; Johnson, 1974) which allow for a simulation of the real experiment by following a given number of neutron histories. By using this

technique a typical statistical error of 1% on the total scattered intensity is generally acceptable.

However, in special cases such as diffraction from gases at high pressure where the contribution from the container exceeds 30% of the total intensity (Fredrikze, 1987) or can reach values of 80-90% (Bellissent-Funel, Buontempo, Petrillo & Ricci, 1989), an accuracy as high as 0·1% in the data reduction is needed to obtain an accuracy of a few percent in the corrected intensity due to single-scattering processes from the sample only. In these cases, the crucial point is the subtraction of the cell contribution from the measured total intensity since multiple processes taking place between sample and cell and into the cell itself, although non-negligible, represent in any case a modest contribution.

Having in mind this kind of experiment, we developed an *ad hoc* data analysis procedure with the aim of minimizing the errors introduced by the subtraction of the container and taking into account absorption and higher-order scattering processes involving the container itself. A numerical simulation of the measured intensities has been set up that allows for the calculation of proper parameters occurring in the analysis procedure, thus obtaining the intensity of single-scattering processes in the sample only. By such a numerical approach both the cases of isotropic and non-isotropic scatterers can be treated; in the latter case a rough knowledge of the angular dependence of the cross section is required as input in the calculation. Finally, inhomogeneities of the incoming beam with respect to the finite dimensions of the sample can be easily taken into account if a model for the beam shape is available.

As a check, the present procedure has been applied to the case of standard scatterers for which MC (Meardon, 1973; Johnson, 1974) and Blech & Averbach (1965) calculations are available. The behaviour of the cell contribution and multiple scattering is discussed for titanium–zirconium and vanadium containers as a function of cell thickness, sample radius, sample linear attenuation coefficient and scattering angle at an incoming neutron wavelength of 0·7 Å.

2. Data analysis

In a neutron diffraction experiment from disordered samples, the most widely used geometry is the cylindrical one as no preferred symmetry axis is present in the sample. Such a geometry is particularly suitable for instance when one studies gaseous or liquid samples under high hydrostatic pressures. In the present analysis, the container will be assumed to be cylindrical in shape and of finite thickness, *i.e.* a non-negligible thickness in terms of attenuation effects and multiple scattering within the wall and the wall and the sample. The latter is necessary when

dealing with containers contributing to the total scattered intensity (sample plus cell) for a fraction greater than 10%. In such experimental conditions, a very high accuracy in subtracting the cell contribution is needed. In particular, an accuracy of 0·1% is necessary to obtain a static structure factor affected by an error of 1% when the cell contribution is of the order of 90% of the total scattered intensity.

At present, approaches based on MC simulation allow for a complete description of the scattering problem in such cases. In a recent experiment on krypton (Fredrikze, 1987) in which the scattering from the cell contributed to 30% of the total intensity, a MC technique has been applied to take into account the multiple scattering. The attenuation of the sample intensity due to the cell was calculated only for single scattering, using numerical integration. However, the accuracy of 1% in the total scattered intensity provided by MC simulation must be carried further, thus increasing the computation time if one decides to calculate all the corrections using such a technique.

Moreover, it must be noted that the calculation of the intensity due to the cell and the evaluation of multiple scattering, in the presence of the sample, suffer from various inaccuracies other than the statistical ones. Indeed the typical wall thickness of the container is of the order of 0·1 cm with an accuracy no better than a few percent, while the total cross sections are known with an absolute error of about 1%. Therefore the direct calculation of the cell contribution is expected to have a sizeable error.

To deal with the above problems, we developed a new procedure that allows for handling the data by using experimentally measured intensities properly corrected by calculated quantities.

The notation employed throughout the present section is reported in Table 1. To simplify the presentation of the following analysis of the experimental data, double-scattering intensities only will be written in the formulae without any lack of generality; the numerical calculation of the parameters appearing in the theory can be done by including higher-order multiple-scattering contributions with a small increase in the computation time. Moreover, for the sake of simplicity, the angular dependence of the intensities is not explicitly reported in the following relationships.

In a typical diffraction experiment employing a monochromatic beam five sets of measurements are performed: scattering from the cell filled with the sample, scattering from the empty cell, scattering from a full absorber (a cadmium rod having the same height as the sample and a radius equal to the external radius of the cell), scattering from the environment obtained by removing sample and cell, and scattering from a vanadium rod having the same height as the sample and a radius equal to the internal radius of the cell. Neglecting inelastic contributions, the measured

Table 1. *Experimental and calculated neutron scattering intensities* [*see* (9) *and* (10)] *and calculated attenuation and transmission coefficients* [*see* (11) *and* (12)]

Intensities given by (10) are written for $n = 2$ scattering events.

I_{s+c}^{exp} experimental intensity from the cell filled with sample.
I_c^{exp} experimental intensity from the empty cell.
I_V^{exp} experimental intensity from a vanadium standard.
I_{vac}^{exp} experimental intensity without sample and container.
I_{abs}^{exp} experimental intensity from a full absorber.
I_s single-scattering intensity from the sample.
I_{ss} double-scattering intensity from the sample.
I_{sc} double-scattering intensity between sample and cell.
I_{cs} double-scattering intensity between cell and sample.
I_c^0 single-scattering intensity from the empty cell.
I_{cc}^0 double-scattering intensity from the empty cell.
I_c^s single-scattering intensity from the filled cell.
I_{cc}^s double-scattering intensity from the filled cell.
I_V single-scattering intensity from vanadium standard.
I_{VV} double-scattering intensity from vanadium standard.
I_{s+c}^B background intensity for the sample plus cell measurement.
I_c^B background intensity for the empty cell measurement.
I_V^B background intensity for vanadium standard measurement.
T_{s+c}^B transmission of sample plus cell.
T_c^B transmission of empty cell.
T_V^B transmission of vanadium standard.
T_s sample attenuation coefficient accounting for the effects due to both sample and cell.
T_V vanadium standard attenuation coefficient.

intensities due to the cell filled with the sample and to the empty cell can be written respectively as:

$$I_{s+c}^{exp} = I_s + I_{ss} + I_{sc} + I_{cs} + I_c^s + I_{cc}^s + I_{s+c}^B \quad (1a)$$

and

$$I_c^{exp} = I_c^0 + I_{cc}^0 + I_c^B, \quad (1b)$$

by assuming that the experimental intensities I_{s+c}^{exp} and I_c^{exp} have already been corrected for detector efficiency and normalized to a given value of monitor counts. It has to be noted that the intensities appearing in (1a) and (1b) contain the appropriate attenuation as suffered by neutrons in crossing both the sample and the cell. Background intensities appearing in (1a) and (1b) are given by

$$I_{s+c}^B = I_{abs}^{exp} + T_{s+c}^B (I_{vac}^{exp} - I_{abs}^{exp}) \quad (2a)$$

and

$$I_c^B = I_{abs}^{exp} + T_c^B (I_{vac}^{exp} - I_{abs}^{exp}). \quad (2b)$$

Provided a numerical estimate of the transmission factors appearing in (2a) and (2b) (see the following section) as accurate as few in a thousand (apart from errors due to sizes and cross sections), subtraction of background I_{s+c}^B and I_c^B is straightforward by using the experimental intensities I_{vac}^{exp} and I_{abs}^{exp}. The subtraction of the cell contribution, which is a critical point, can be done by defining the ratio between the

intensities scattered by the cell with and without the sample, i.e.

$$\gamma = (I_c^s + I_{cc}^s)/(I_c^0 + I_{cc}^0). \quad (3)$$

By combination of (1b) and (3), (1a) can be written as

$$I_{s+c}^{exp} - I_{s+c}^B - \gamma(I_c^{exp} - I_c^B) = I_s + I_{ss} + I_{sc} + I_{cs}. \quad (4)$$

One may account for the double- (multiple-) scattering contributions appearing on the right-hand side of this last equation by calculating the ratio (Fredrikze, 1987)

$$m = \lim_{Q \to \infty} [(I_{ss} + I_{sc} + I_{cs})/(I_s)] \quad (5)$$

at high values of the momentum transfer Q. Introducing the multiple-scattering parameter m in (4), the intensity from the sample due to single-scattering processes only can be written as

$$I_s = [I_{s+c}^{exp} - I_{s+c}^B - \gamma(I_c^{exp} - I_c^B)]$$
$$- m/(m+1)[I_{s+c}^{exp} - I_{s+c}^B - \gamma(I_c^{exp} - I_c^B)]_{Q \to \infty} \quad (6)$$

where *measured quantities* are related by the *two calculated parameters* γ and m and the transmissions.

Indeed, γ and m have been deduced by a numerical calculation of the intensities appearing in the right-hand side of (1a) and (1b) (see §3) following a procedure quite similar to that suggested by Blech & Averbach (1965), the main difference arising from the inclusion of a cell with finite thickness. In such a way, contributions coming from the non-convex volume of the container are taken into account thus making the full system no more homogeneous.

It has to be noted that when the ratio γ is close to unity, i.e. in the case of a weak sample, it is affected by an error smaller than that in the calculated intensities, other errors being negligible. This follows directly both from the definition of γ and the numerical procedure employed in calculating the intensities. The error introduced in the subtraction of the cell contribution is thus governed by the error in γ, which can be reduced to 0·1–0·2%, and by the statistical error affecting the measured intensity I_c^{exp}. The numerical uncertainty affecting the calculation of the background transmissions is a less-critical point considering that the scattering from the environment (I_{vac}^{exp}) and from the absorber (I_{abs}^{exp}) are generally very low as compared to the cell and sample scattering. A numerical accuracy of about 1% in m is possible, even though in the case of a low-scattering sample, a rougher estimate of this parameter does not significantly increase the error in the single-scattered intensity I_s [(6)]. It should be noted that, while the error in γ is dominated by that in the calculated single-scattering intensities, which are greater than the multiple ones, the error in m is related to that in multiple-process intensities which are known less accurately.

The single-scattering intensity given by (6) still contains the attenuation of the neutron beam due to the cell walls and to the sample at different angles. Such an attenuation factor can be calculated numerically as in the case of background transmissions.

From the intensity corrected for the attenuation, the differential cross section can be obtained by normalization to the vanadium standard as

$$d\sigma/d\Omega = (d\sigma/d\Omega)_V (I_s T_V)/(I_V T_s) \qquad (7)$$

where $(d\sigma/d\Omega)_V = \sigma_V^{inc}/4\pi$, σ_V^{inc} being the incoherent cross section of vanadium. I_V is deduced by the measured intensity on the vanadium rod by applying the same procedure leading to (8) which in this case is written as

$$I_V = I_V^{exp} - I_V^B - m_V/(m_V+1)[I_V^{exp} - I_V^B] \qquad (8)$$

where $I_V = I_{abs}^{exp} + T_V^B(I_{vac}^{exp} - I_{abs}^{exp})$ and $m_V = I_{VV}/I_V$. I_{vac}^{exp} and I_{abs}^{exp} have the same meaning as in the case of the sample except that the cadmium rod should have the same radius as the vanadium rod, i.e. the inner radius of the cell. The evaluation of I_V as given by (8) can be compared directly with that obtained using other procedures (Paalman & Pings, 1962; Blech & Averbach, 1965; Meardon, 1973) and thus one can obtain more information on the validity of the present approach.

3. Numerical calculation and discussion of the errors

As seen in the previous section, the parameters appearing in the data analysis are γ, which appears in the cell subtraction, m, the multiple scattering factor, background transmissions and sample attenuation. Evaluation of these parameters implies the calculation of single- and multiple-scattering intensities entering in the diffraction experiment.

In Fig. 1 a section of the cell perpendicular to the cylinder axis is presented showing all single-scattering processes which can take place in the sample or in the cell, $L_I(\mathbf{r})$ and $L_F(\mathbf{r})$ being the path lengths of the incoming and scattered neutron beams. Such path
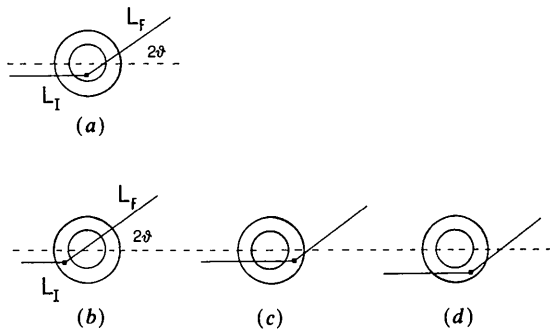
lengths are functions of the point coordinate $\mathbf{r}$, as they are the sum of paths within the cell and/or the sample. The origin of the coordinate system is fixed at the center of the cylinder with the z axis along the axis of the cylinder.

Assuming a unitary incoming neutron flux J_0, the total intensity for single scattering and for multiple scattering of order n $(n > 1)$, in neutrons per solid angle and unit time, can be written respectively as

$$I_\alpha^1 = N_\alpha (d\sigma/d\Omega)_\alpha \int_{V_\alpha} d\mathbf{r} \exp(-X_I - X_F), \qquad (9)$$

$$I_{\alpha 1...\alpha n}^n = \prod_{i=1}^{n} \left[N_{\alpha i}(d\sigma/d\Omega)_{\alpha i} \int_{V_{\alpha i}} d\mathbf{r}_i 1/ \prod_{j=1}^{n-1} L_j^2 \right.$$

$$\left. \times \exp\left(-X_I - X_F - \sum_{k=1}^{n-1} X_k\right)\right], \qquad (10)$$

where the index α refers to the sample or the cell and V_α is the corresponding volume. N_α is the number density and $(d\sigma/d\Omega)_\alpha$ the differential cross section. X_I and X_F are the path integrals of the total linear attenuation coefficient along L_I and L_F respectively and X_i is the integral along the path L_i between ith and $(i+1)$th events. Of course in the calculation of the path integrals the variation of the linear attenuation coefficient across the boundaries is taken into account. Equation (10) is the exact integral form of the transport equation for the neutron flux due to n-scattering processes (Sears, 1975). In Fig. 2, for the sake of simplicity, all the possible double-scattering events taking place in the system cell plus sample are shown.

Fig. 1. Section of the cell perpendicular to the cylinder axis showing all single-scattering processes taking place (a) within the sample and (b), (c), (d) within the cell wall.
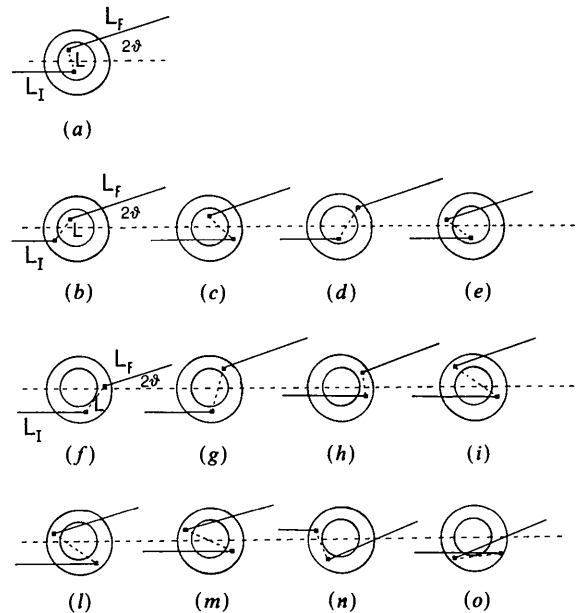
Fig. 2. Section of the cell perpendicular to the cylinder axis showing all double-scattering processes taking place (a) within the sample, (b), (c), (d), (e) between sample and cell and (f), (g), (h), (i), (l), (m), (n), (o) within the cell.

Finally, the factor taking into account the attenuation suffered by the neutron beam during the single-scattering process at the different scattering angles can be written as

$$T = 1/V_\alpha \int_{V_\alpha} \mathrm{d}\mathbf{r} \exp(-X_I - X_F). \qquad (11)$$

These quantities, which contain an angular dependence, are the ratio between the measured intensities and the theoretical ones, and define both a sample and a cell factor accounting for the attenuation during the scattering processes shown respectively in Fig. 1(a) and in Figs. 1(b)-(d). We note that the present definition of sample and cell attenuations is the same as that of the cylindrical absorption factors as given by Paalman & Pings (1962): the sample attenuation is the coefficient called $A_{s,sc}$, while the cell attenuation is the $A_{c,sc}$ coefficient, meaning respectively absorption factor for scattering in the sample with absorption in both sample and cell and absorption factor for scattering in the cell with absorption in both the sample and cell.

The background transmission of the filled or empty cell can be calculated, as usual, by using the following relationship:

$$T^B = 1/(2R_c) \int_{-R_c}^{R_c} \mathrm{d}y \exp[-X(y)] \qquad (12)$$

where $X(y)$ is the appropriate path integral of the total linear attenuation coefficient along a straight line parallel to the direction of the incoming neutron beam and R_c is the cell radius. Although in principle (12) differs from (11), the use of the latter at zero scattering angle yields results numerically very close to those calculated from (12) in most cases.

The calculation of the quantities given in (9) and (11) implies an integration over three dimensions, immediately reducible to two, while an integration over $3n$ dimensions is required in (10). In addition, linear attenuation coefficients and path lengths present in these equations must be evaluated by taking into account the medium discontinuity in crossing the boundary between the cell wall and the sample. Path lengths associated with multiple processes can easily be calculated by searching for the interception points between the straight lines of the neutron path and the cylindrical surfaces of both the cell and the sample.

The calculation of these integrals can be afforded by using a MC integration procedure in which a random sampling of the integration volume is performed. Such a MC procedure should, however, be considered with some care. The first problem which arises in performing integrals in $3n$-dimensional space by using the MC method is that the correlations, always present in random-number-generator routines (Press, Flannery, Tenkolsky & Vetterling, 1986) produce a non-uniform sampling of the appropriate

volumes. Moreover, the absolute accuracy of 0·1% seems to be too high a demand. To deal with these problems, it must be observed that the highest accuracy should be obtained for the γ coefficient which is an intensity ratio. Therefore, a small error in γ can be obtained if the numerator and denominator errors cancel each other. To establish this condition, the integrations over the cell volume necessary to calculate the I_c^s, I_{cc}^s, I_c^0, I_{cc}^0 terms have been performed by using a fixed random sampling of such a volume. In this way the error due to the limited number of points used in the MC procedure is reduced when the intensity ratio is considered. Indeed, if $\Delta\varepsilon$ is the relative error in estimating I_c^0 or I_c^s, the error in estimating γ is $\Delta\gamma \simeq \Delta\varepsilon(1-\gamma)$ so that, when γ is not far from unity, the error in it is appreciably reduced compared with the result obtained when the integrals are evaluated as independent quantities. In addition, when γ is small compared with 1, the contribution of the cell to the total scattered intensity is smaller and the accuracy of γ need not be so great. The above argument also holds when we consider the angular dependence of all the quantities or when different samples having the same size are considered, that is the ratio of two intensities produced by the present procedure is much better defined than the intensities themselves. Finally, in order to reduce the systematic errors due to the correlation introduced by the random-number generator, we used several independent random sequences in carrying out each integration.

To perform the $3n$-dimensional integration necessary to determine the multiple-scattering contribution, we sampled randomly the $(n-1)$ distances between the n points inside the integration volume. In this way, the required computation time is almost the same for single as well as for any order multiple scattering, although the relative error on each integral increases with the order of the process. Thus, using the present approach, each scattering order gives an almost constant contribution to the total error. The accuracy on each intensity term can obviously be improved by increasing the number of points randomly drawn inside the volume. As a consequence the statistical error on m and γ can progressively be reduced. Several trials have been done by varying the number of points in the integration volume from 10^5 to 5×10^6. It was found that, for more than 5×10^5 points, convergence of the single-scattering intensity values is reached with relative variations of 0·2% from the asymptotic result. By using 2×10^5 points, statistical errors in γ and m are about 0·1–0·2% and 1% respectively when the linear attenuation coefficient of the sample is not too high. This result can be considered rather satisfactory and it is attainable with a relatively small computation time. The computer time has been estimated by using an IBM 3090 system and it was found that all the integrals contributing

Table 2. *Linear attenuation coefficients employed in the calculations*; $\mu^{scat} = N\sigma^{scat}$ *and* $\mu^{abs} = N\sigma^{abs}$, N *being the number density*, σ^{scat} *and* σ^{abs} *being respectively scattering and absorption cross sections*

	μ^{scat} (cm^{-1})	μ^{abs} (cm^{-1}) $\lambda = 0.7$ Å	μ^{abs} (cm^{-1}) $\lambda = 1$ Å	μ^{abs} (cm^{-1}) $\lambda = 10$ Å
V	0·357	0·144	0·206	2·06
Ni	0·386	—	0·00	0·00
Ti–Zr	0·254	0·086	—	—

to second-order scattering could be calculated in 10^{-4} s of central processing unit (CPU) time per sampled point. This implies 1 min CPU time for 5×10^6 points per integral. A further check of the numerical accuracy of the results has been done by carrying out the calculation in a double-precision definition of all the relevant variables. By using the same fixed random sampling of the integration volume, no variation in changing from single to double precision has been found. Finally, the computation procedure has been checked in cases when an analytical integration can be carried out. It was found that numerical and analytical results were equal within 0·2–0·4%, using 10^5 points in the integration volume, as expected from the other checks we have performed.

4. Results and discussion

Firstly, results on standard scatterers obtained by running the present numerical program have been compared with those by other approaches. Typical tests, already used in MC simulations (Meardon, 1973), are the vanadium rod and a hypothetical sample having the incoherent cross section of nickel and no absorption. In Table 2, linear attenuation coefficients related to scattering (μ^{scat}) and true absorption (μ^{abs}) cross sections employed as input of present calculations are reported. In Figs. 3(a) and (b), results from these two cases are shown in comparison with MC data (Meardon, 1973) and, as we can see, the overall quantitative agreement is very good. Because of the integration method we employed, our data do not exhibit random fluctuations which are instead present in the MC ones, though the computation time is of the same order of magnitude in both the approaches.

The present program can also be employed to reproduce the Blech & Averbach (1965) calculations of the coefficient δ for secondary scattering which is defined as

$$\delta = (\sigma^{tot} I^2)/(\sigma^{scat} I^1),$$

σ^{scat} and σ^{tot} being the scattering and total cross sections of the homogeneous cylindrical system respectively. In Blech & Averbach (1965), such a coefficient is calculated under the assumption of isotropic scattering, which implies the substitution $d\sigma/d\Omega \to \sigma/4\pi$, by taking a series expansion of the
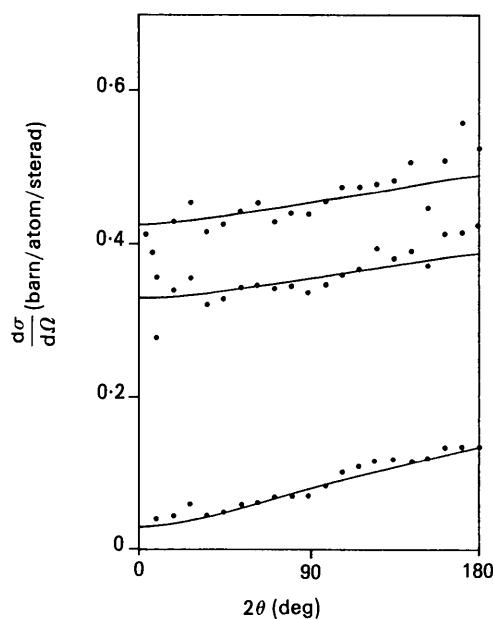
(a)
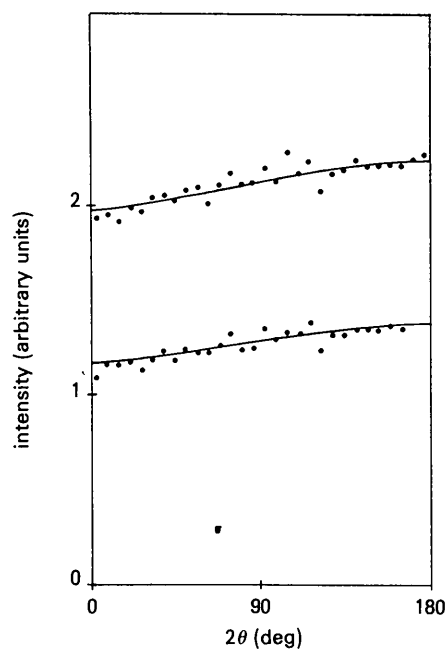
(b)

Fig. 3. (a) Differential cross section of a vandanium rod obtained by present approach (full line) as compared with MC results (dots) (Meardon, 1973). Starting from the lowest curve, data refer to the total differential cross section at $\lambda = 10$ Å, single-scattering and total differential cross sections both at $\lambda = 1$ Å. (b) Scattering intensity of a nickel rod with no absorption obtained by the present approach (full line) as compared with MC results (dots) (Meardon, 1973). The upper curve is the total intensity while the lower one is the single-scattering intensity.

integrands in (9) and (10) and averaging over the scattering angles. Though such an approximation is not too severe when the total linear attenuation coefficient $\mu = \mu^{scat} + \mu^{abs}$ is not too high, it has already been recognized (Meardon, 1973) that δ is a slightly decreasing function of the scattering angle as a consequence of the fact that I^1 is an increasing function of the scattering angle while I^2 is almost constant. In Fig. 4, δ by Blech & Averbach (1965) and by the present calculation is shown as a function of the scattering angle at the values $\mu R = 0.5$ and $R/h = 0.2$ (R and h being radius and height of the cylinder).

The behaviour of γ and m defined by (3) and (5) has been investigated as a function of (a) the scattering angle 2θ, (b) the linear attenuation coefficient of the sample μ, (c) the cell thickness t and (d) the sample radius R. Two different values of the linear attenuation coefficient of the cell, corresponding to vanadium and Ti-Zr null-matrix alloy, have been chosen (see Table 2). The linear attenuation coefficient μ of the sample has been evaluated by assuming a zero absorption cross section, the attenuation thus being due to scattering processes only. The calculations have been carried out at an incoming neutron wavelength of 0.7 Å by fixing the height h of the cylinder ($h = 5$ cm) and assuming isotropic scattering and a homogeneous beam. In each case 2×10^5 points within the integration volume were employed. Results for m and γ are reported in Tables 3 and 4. As we can see from Table 3, m shows quite a smooth dependence on both μ and 2θ. In Fig. 5, the behaviour of m as a function of the scattering angle is reported at different values of μ for two R/h ratios in the two cases of vanadium and Ti-Zr cells. A definite angular dependence of m is seen when

Table 3. *Double-scattering parameter* m (%) *at different values of the scattering angle, the sample attenuation coefficient* μ, *at two values of the cell thickness* t *and three* R/h *ratios, for vanadium and* Ti-Zr *cells*

	Vanadium cell					
	$t = 0.05$ cm			$t = 0.1$ cm		
$2\theta(°)$	10	50	100	10	50	100
μ (cm⁻¹)						
0.1	11.0	11.0	11.0	15.3	15.3	15.3	
0.2	16.3	16.3	16.3	20.3	20.3	20.3	
0.3	21.1	21.2	21.1	24.9	25.0	24.9	$R/h = 0.1$
0.4	25.6	25.7	25.6	29.2	29.3	29.2	
0.5	29.8	30.0	29.7	33.3	33.4	33.1	
0.1	14.3	14.3	14.3	18.2	18.2	18.2	
0.2	22.5	22.5	22.4	26.3	26.3	26.2	
0.3	29.6	29.7	29.4	33.3	33.3	33.1	$R/h = 0.2$
0.4	35.9	36.0	35.4	39.5	39.6	39.0	
0.5	41.4	41.6	40.6	45.0	45.2	44.1	
0.1	16.9	16.9	16.9	20.4	20.4	20.4	
0.2	27.1	27.1	26.9	30.4	30.5	30.2	
0.3	35.6	35.6	35.0	38.8	38.8	38.2	$R/h = 0.3$
0.4	42.6	42.7	41.5	45.8	45.8	44.6	
0.5	48.6	48.7	46.8	51.8	51.8	49.8	

	Ti-Zr cell					
	$t = 0.05$ cm			$t = 0.1$ cm		
$2\theta(°)$	10	50	100	10	50	100
μ (cm⁻¹)						
0.1	9.61	9.61	9.61	12.8	12.8	12.8	
0.2	14.9	14.9	14.9	17.9	17.9	17.8	
0.3	19.8	19.8	19.7	22.6	22.6	22.5	$R/h = 0.1$
0.4	24.4	24.5	24.3	27.0	27.0	26.8	
0.5	28.6	28.8	28.5	31.0	31.1	30.8	
0.1	13.1	13.1	13.1	16.0	16.0	16.0	
0.2	21.3	21.4	21.3	24.1	24.2	24.1	
0.3	28.5	28.6	28.3	31.3	31.3	31.0	$R/h = 0.2$
0.4	34.8	34.9	34.4	37.5	37.6	37.0	
0.5	40.4	40.7	39.7	43.1	43.2	43.2	
0.1	15.8	15.8	15.7	18.4	18.4	18.3	
0.2	26.1	26.1	25.9	28.5	28.6	28.3	
0.3	34.5	34.6	34.1	37.1	37.1	36.4	$R/h = 0.3$
0.4	41.6	41.8	40.6	44.0	44.1	43.0	
0.5	47.6	47.9	45.7	50.2	50.2	48.0	

$\mu > 0.1$ in the whole range of R/h we have studied; in particular, m shows a maximum at intermediate values of the scattering angle. Finally, it should be observed that m is dependent on both μ^{scat} and μ^{abs}, the relevant parameter being however the total μ. As has been stated, the present results are obtained for a non-absorbing sample but they can easily be generalized to the non-zero absorption case by studying the dependence on μ of the higher order intensities [see (10)]. Indeed, the following relationships hold for instance in the case of double-scattering processes:

$$I_{ss}(\mu^{abs}; \mu^{scat}) = [\mu^{scat}/(\mu^{abs} + \mu^{scat})]^2$$
$$\times I_{ss}(0; \mu^{abs} + \mu^{scat}) \qquad (13a)$$

$$I_{sc}(\mu^{abs}; \mu^{scat}) = \mu^{scat}/(\mu^{abs} + \mu^{scat})$$
$$\times I_{sc}(0; \mu^{abs} + \mu^{scat}) \qquad (13b)$$

$$I_{cc}(\mu^{abs}; \mu^{scat}) = I_{cc}(0; \mu^{abs} + \mu^{scat}) \qquad (13c)$$
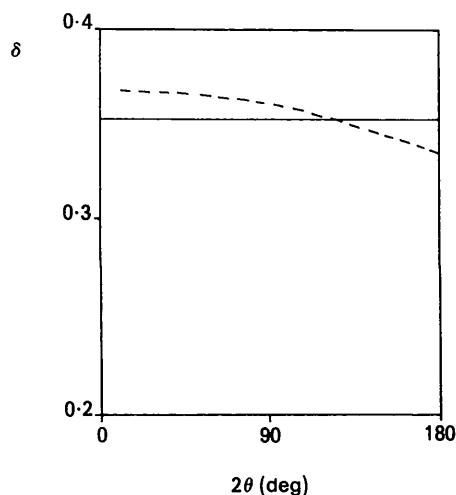

Fig. 4. Coefficient for secondary scattering δ as a function of the scattering angle, calculated for a cylindrical sample having $\mu R = 0.5$ and $R/h = 0.2$. The full line is by Blech & Averbach (1965).

Table 4. γ coefficient at different values of the scattering angle, the sample attenuation coefficient μ, at two values of the cell thickness t and three R/h ratios, for vanadium and Ti–Zr cells

Vanadium cell

	$t = 0.05$ cm			$t = 0.1$ cm			
$2\theta(°)$	10	50	100	10	50	100	
μ (cm^{-1})							
0·1	0·943	0·943	0·945	0·945	0·947	0·950	
0·2	0·890	0·891	0·896	0·895	0·898	0·905	
0·3	0·842	0·844	0·852	0·849	0·853	0·864	$R/h = 0.1$
0·4	0·797	0·800	0·812	0·807	0·811	0·827	
0·5	0·756	0·760	0·776	0·768	0·773	0·794	
0·1	0·883	0·886	0·891	0·887	0·890	0·897	
0·2	0·784	0·789	0·804	0·791	0·798	0·814	
0·3	0·699	0·708	0·733	0·710	0·719	0·746	$R/h = 0.2$
0·4	0·627	0·638	0·675	0·640	0·653	0·691	
0·5	0·565	0·579	0·627	0·581	0·596	0·646	
0·1	0·829	0·834	0·845	0·831	0·837	0·851	
0·2	0·694	0·705	0·732	0·698	0·711	0·742	
0·3	0·588	0·604	0·648	0·594	0·613	0·662	$R/h = 0.3$
0·4	0·503	0·524	0·586	0·511	0·535	0·602	
0·5	0·435	0·462	0·540	0·446	0·475	0·557	

Ti–Zr cell

	$t = 0.05$ cm			$t = 0.1$ cm			
$2\theta(°)$	10	50	100	10	50	100	
μ (cm^{-1})							
0·1	0·943	0·944	0·945	0·947	0·947	0·950	
0·2	0·891	0·892	0·896	0·898	0·899	0·904	
0·3	0·843	0·845	0·851	0·852	0·854	0·863	$R/h = 0.1$
0·4	0·799	0·801	0·811	0·811	0·813	0·827	
0·5	0·758	0·761	0·775	0·772	0·776	0·793	
0·1	0·885	0·887	0·891	0·889	0·891	0·897	
0·2	0·787	0·791	0·804	0·795	0·799	0·813	
0·3	0·703	0·709	0·732	0·715	0·722	0·745	$R/h = 0.2$
0·4	0·632	0·640	0·674	0·647	0·655	0·689	
0·5	0·571	0·581	0·627	0·589	0·599	0·644	
0·1	0·831	0·835	0·844	0·834	0·839	0·850	
0·2	0·698	0·706	0·731	0·704	0·713	0·740	
0·3	0·592	0·606	0·648	0·601	0·615	0·659	$R/h = 0.3$
0·4	0·508	0·526	0·586	0·520	0·538	0·599	
0·5	0·441	0·464	0·539	0·455	0·478	0·553	

where the left hand side of these equations gives the intensities for the absorbing sample.

We can see from Table 4 that γ exhibits uniform trends as a function of all the parameters so that reasonable estimates can also be derived by interpolation for cases other than those reported in the tables. It must be remarked that γ is independent of the ratio μ^{scat}/μ^{abs} of the sample, as can be seen from (13c). In Figs. 6(a) and (b), γ versus the scattering angle is plotted at different values of μ and R/h for the two cells. It is seen from this figure that γ increases monotonically as a function of scattering angle in the examined range. In Fig. 7 present values of γ as a function of μR in the case of the vanadium container are shown in comparison with the results obtained in the 'thin-walled' limit (Fredrikze, 1987). Examining this figure in the region of interest ($\mu R < 0.2$ and $0.8 < \gamma < 1$), appreciable disagreement between the two calculations is found (differences up to 3%) when the sample radius is not too large.
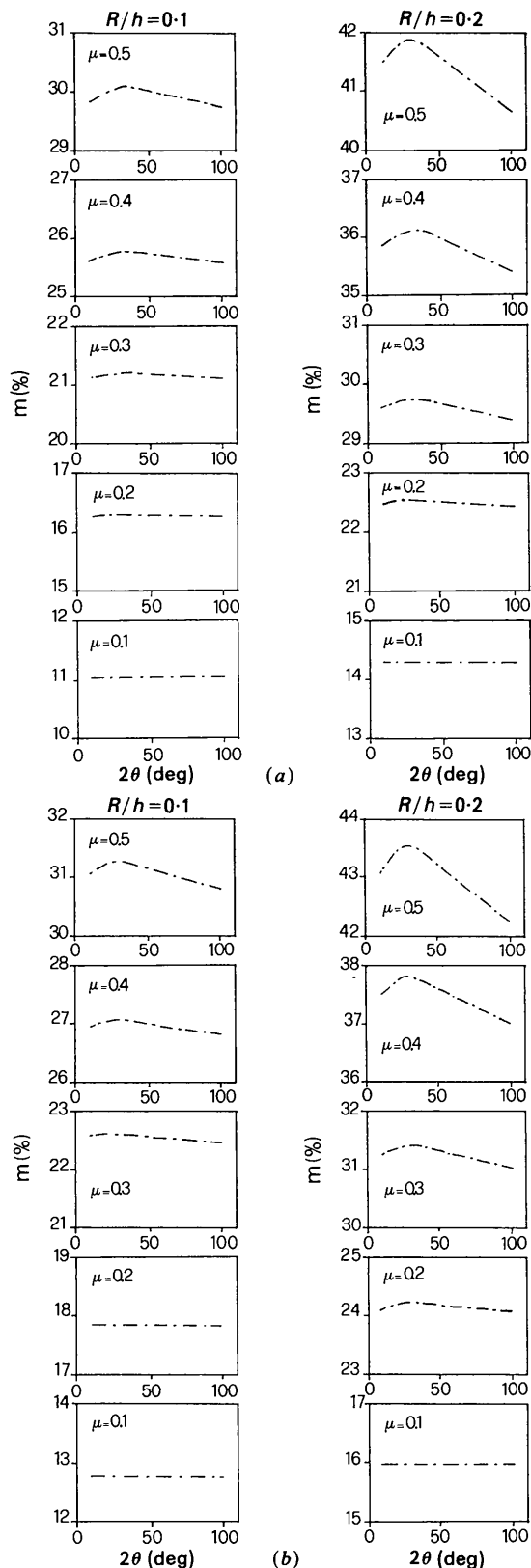

Fig. 5. Double-scattering coefficient m (%) as a function of the scattering angle at several values of the sample attenuation coefficient μ and for two R/h ratios. (a) Vanadium cell of 0·05 cm thickness; (b) Ti–Zr cell of 0·10 cm thickness.

The effect of the transvérse shape of the incoming beam on γ has also been analysed. We calculate γ by assuming a Gaussian-shaped beam having a full width at half maximum W such that $W/R = 2$. Results are shown in Fig. 6(b) in comparison with those obtained in the case of a homogeneous beam. The most important conclusion we can make from this figure is the enhancement of the angular dependence of γ due to the finite width of the beam. Therefore, when an accurate data analysis is needed, such an effect has to be taken into account by a proper measurement of the beam profile.

The dependence of the two parameters γ and m on the height of the cylinder has also been investigated. Calculations have been done by fixing the

radius of the sample ($R = 1$ cm) in the case of the vanadium cell having two different thickness values ($t = 0.05$ and 0.10 cm). As an example, we report in Tables 5(a) and (b) results obtained at the scattering angle $2\theta = 50°$ and at three values of the linear attenuation coefficient of the non-absorbing sample. Effects of non-zero absorption can be taken into account by referring to $(13a)$-$(13c)$. As expected, m shows a marked dependence on the height of the specimen (Blech & Averbach, 1965), while only a weak dependence is found for γ.

Finally, we have treated the case of a non-isotropic scatterer to investigate the effect due to deviations from isotropy on the parameters γ and m. A simulation of a gaseous sample of krypton at a pressure of about 100 MPa has been done by using the Percus–Yevick approximation in order to deduce a static structure factor as input to the calculation. A Ti–Zr cell having 1 cm internal diameter and 0.2 cm wall thickness was employed in the simulation. For purposes of comparison, the same sample has also been investigated with the hypothesis of isotropic scattering. In view of the present numerical procedure, the two sets of data can be compared safely and what we found is that the isotropic approximation gives a good description of both γ and m within the present accuracy (0.1%). Therefore it can be generally employed for a wide class of scattering problems without any special care.

The data reduction and the numerical procedure we have described have already been successfully applied to the analysis of neutron diffraction from gaseous Xe and He–Xe mixtures contained in a Ti–Zr high-pressure cell (Bellissent-Funel, Buontempo, Petrillo & Ricci, 1989).
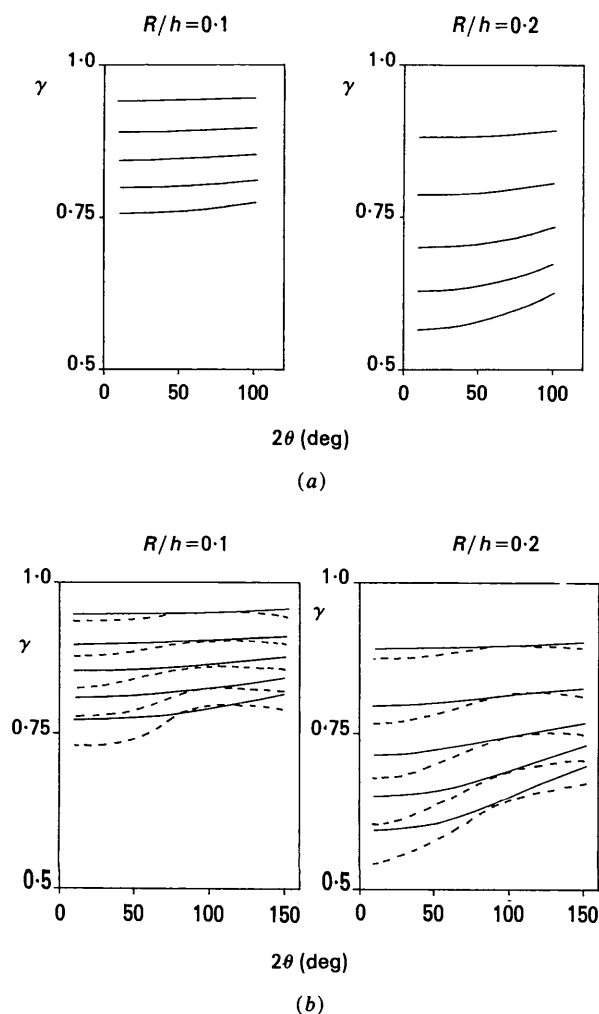

Fig. 6. γ coefficient as a function of the scattering angle at several values of the sample attenuation coefficient μ (0.5, 0.4, 0.3, 0.2, 0.1 starting from the lowest curve) and for two R/h ratios. (a) Vanadium cell of 0.05 cm thickness; (b) Ti–Zr cell of 0.10 cm thickness. For comparison purposes γ as calculated for a Gaussian beam having $W = 1$ cm at $R/h = 0.1$ and $W = 2$ cm at $R/h = 0.2$ is shown (dashed lines).
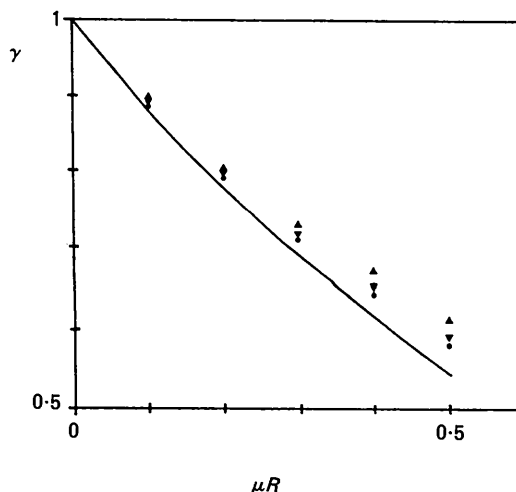

Fig. 7. γ coefficient *versus* μR at zero scattering angle and at three values of the vanadium cell thickness: $t = 0.05$ cm ($\bullet$); $t = 0.10$ cm ($\blacktriangledown$); $t = 0.20$ cm ($\blacktriangle$). The full line is the result obtained in the 'thin-walled' limit (Fredrikze, 1987).

Table 5. *Calculated parameters versus the sample height* (h), *at a fixed radius* $R = 1$ cm, *at different values of the sample attenuation coefficient* μ *and at two values of the vanadium cell thickness* t

Results refer to the scattering angle $2\theta = 50°$. (a) Double-scattering parameter m (%); (b) γ coefficient.

(a) Vanadium cell; double-scattering parameter m

	h (cm)				
μ (cm^{-1})	1	3·33	5	10	
0·1	8·34	12·9	14·3	16·3	
0·3	18·3	27·1	29·7	33·8	$t = 0·05$ cm
0·5	26·4	38·1	41·6	47·6	
0·1	10·4	16·5	18·2	20·8	
0·3	20·3	30·4	33·3	37·9	$t = 0·10$ cm
0·5	28·4	41·3	45·2	51·7	

(b) Vanadium cell; γ coefficient

	h (cm)				
μ (cm^{-1})	1	3·33	5	10	
0·1	0·887	0·886	0·886	0·885	
0·3	0·710	0·708	0·708	0·706	$t = 0·05$ cm
0·5	0·582	0·580	0·579	0·578	
0·1	0·892	0·891	0·890	0·889	
0·3	0·722	0·720	0·719	0·717	$t = 0·10$ cm
0·5	0·600	0·597	0·596	0·594	

The present program will be made available to interested parties on request.

References

BELLISSENT-FUNEL, M. C., BUONTEMPO, U., PETRILLO, C. & RICCI, F. P. (1989). *Phys. Rev. A*, **40**, 7346–7354.
BISCHOFF, F. G., YEATER, M. L. & MOORE, W. E. (1972). *Nucl. Sci. Eng.* **48**, 266–281.
BLECH, I. A. & AVERBACH, B. L. (1965). *Phys. Rev. A*, **137**, 1113–1116.
COPLEY, J. R. D. (1974). *Comput. Phys. Commun.* **7**, 289–317.
COPLEY, J. R. D. (1981). *Comput. Phys. Commun.* **21**, 431–436.
COPLEY, J. R. D., VERKERK, P., VAN WELL, A. A. & FREDRIKZE, H. (1986). *Comput. Phys. Commun.* **40**, 337–342.
FREDRIKZE, H. (1987). *Phys. Rev. A*, **36**, 2272–2287.
JOHNSON, M. W. (1974). *UKAEA.* Report AERE-R7682. United Kingdom Atomic Energy Authority.
MEARDON, B. H. (1973). *UKAEA.* Report AERE-R7302. United Kingdom Atomic Energy Authority.
PAALMAN, H. H. & PINGS, C. J. (1962). *J. Appl. Phys.* **33**, 2635–2639.
PRESS, W. H., FLANNERY, B. P., TENKOLSKY, S. A. & VETTERLING, W. T. (1986). *Numerical Recipes.* Cambridge Univ. Press.
SEARS, V. F. (1975). *Adv. Phys.* **24**, 1–45.

Contrast Formation in Synchrotron White-Beam Topographs

By C. A. M. CARVALHO AND Y. EPELBOIN

Laboratoire de Minéralogie-Cristallographie, Universités P. M. Curie (*Paris 6*) *et Paris 7, UA09 CNRS, 4 place Jussieu, 75252 Paris CEDEX 05, France*

Abstract

It is shown theoretically that the contrast of synchrotron white-beam topographs, in most cases, is the superposition of the intensities produced by incoherent point sources situated on the entrance surface of the crystal. This is the reason for the similarity between synchrotron topographs and laboratory translation topographs. It is a consequence of the spectral width of the radiation and of the particle beam size and divergence in the storage ring. Upper and lower bounds are given for the coherence length. The natural collimation of synchrotron radiation and the effect of the source-to-crystal and crystal-to-film distances are taken into account. The results are valid for a large class of synchrotron sources.

I. Introduction

Synchrotron white-beam topography is an attractive technique for the investigation of crystal defects. Some of its advantages over laboratory topographs are imaging of large areas without moving the crystal, and shorter exposure times due to the high intensity of the beam. Many reflections can be recorded simultaneously, and the whole crystal always gives rise to an image, even when it is curved or highly distorted, due to the wide wavelength spectrum.

But synchrotron radiation is rather different from laboratory characteristic line radiation. Also, the distance between source and crystal differs by about two orders of magnitude from laboratory arrangements. This raises the question of the interpretation of the